# Ocean color estimates of particulate organic carbon reservoirs in the global ocean - revisited

Malgorzata Stramska [a, b,*]
Agata Cieszyńska [a, b]

[a]Institute of Oceanology of the Polish Academy of Sciences, Powstańców Warszawy 55, Sopot 81-712, Poland

[b] Department of Earth Sciences, Szczecin University, Mickiewicza 16, Szczecin 70-383, Poland

* corresponding author

Phone: (+48 58) 73 11 600

Fax: (+48 58) 55 12 130

email: mstramska@wp.pl, mstramska@yahoo.com

Index terms: Satellite Sensing, Ocean Color, Climatic Changes, Carbon cycling

This work was supported by the National Science Centre (NCN) in Poland under grant 2011/01/M/ST10/07728 „Global estimates of particulate organic carbon reservoir and export flux in the ocean based on satellite ocean color data". Partial support for MS comes also from the statutory funds of the Institute of Oceanology of the Polish Academy of Sciences (IO PAN).

**Abstract**

We have examined 16 years (1998-2013) of particulate organic carbon (POC) concentrations derived from remotely sensed ocean color. POC concentrations vary spatially from more than 300 mg $m^{-3}$ in the northern North Atlantic in summer to about 20 mg $m^{-3}$ in the oligotrophic South Pacific (16-year global average = 67.7 mg $m^{-3}$). The seasonal variability is weak at lower latitudes and stronger at higher latitudes. The annual mean surface POC concentrations show statistically significant regional trends ($p<0.05$, 95% confidence level), and are decreasing in the North Atlantic and North Pacific and increasing in the South Pacific and Southern Oceans. Global trend is not significant. The 16-year global average water column POC biomass integrated over the euphotic depth, the mixed layer depth, or based on a combination of these two depths is estimated at about 3.97, 3.92, and 5.03 g $m^{-2}$, respectively. Water column integrated biomass shows different spatial and seasonal patterns than the surface POC concentrations, and is increasing in many ocean regions. Globally averaged POC biomass is also increasing. At the same time ocean color data indicate a decrease in the global oceanic productivity (PP). This means that there is a negative trend in the ratio of PP to POC biomass almost everywhere in the ocean. Such a decrease could indicate that the biological pump in the ocean is weakening, but longer time series of the ocean color data are needed to confirm this observation.

## 1. Introduction

The ocean plays an important role in the Earth's carbon cycle. Total amount of carbon stored in the ocean is about 50 times greater than in the atmosphere. It has been estimated that about 50% of the carbon emitted to the atmosphere by fossil fuel burning is sequestered into the oceans (IPCC, 2007). The living phytoplankton component of particulate organic carbon (POC) contributes about 50% of global primary production on the Earth (Behrenfeld et al., 2005).

Biologically driven sequestration of carbon from the atmosphere to the deep sea, called the biological pump, consists of the soft-tissue pump and the carbonate pump where hard tissues are created (e.g., Longhurst and Harrison, 1989). The biological pump

operates in three phases. In the first phase the carbon is fixed into soft or hard tissue by planktonic phototrophs in the euphotic layer of the ocean. Once this carbon is fixed, the organisms either stay in the euphotic zone and are recycled as part of the regenerative nutrient cycle, or continue to the second phase of the biological pump if they sink to the ocean floor. The sinking particles often form aggregates, increasing they sinking velocity (e.g., Honjo et al., 2008; Siegel et al., 2014). Organic carbon in these particles is partly decomposed by bacteria during the sinking process or after the particles settle on the sea floor. In the third phase of the biological pump carbon can be remineralized and used again in primary production. Particles that avoid remineralization are buried in the sediments and may remain there for thousands of years. It is the carbon stored in these particles that is responsible for ultimately lowering atmospheric $CO_2$ concentration (e.g., Siegel et al., 2014).

The biological pump plays an important role in the sequestration of atmospheric $CO_2$, therefore considerable efforts are devoted to quantifying its strength. However, the processes involved in the biological pump are difficult to quantify because they include poorly constrained ecological interactions. Significant attempts have been made to assess various compartments and processes of the oceanic carbon cycle, in particular to quantify the primary production and the so-called f-ratio, a proxy for the strength of the biological pump (e.g., Behrenfeld and Falkowski, 1997; Laws et al., 2000; Behrenfeld et al., 2005; Dunne et al., 2007). Particulate organic carbon (POC) represents only a small portion of the total carbon in the global ocean, but its importance results from a significant contribution to carbon sequestration. Interestingly, unlike other compartments of the global carbon cycle, the size of POC reservoir is small in comparison to POC fluxes in and out of this reservoir. This implies that even small changes in POC reservoir can indicate substantial changes in the related fluxes (e.g., Behrenfeld et al., 2005). Thus, the analysis of the distribution and magnitude of oceanic pool of POC is important for understanding the role of marine biosphere in the global carbon cycle.

To date, several attempts have been made to develop empirical algorithms and to estimate oceanic POC content from ocean color (Stramski et al. 1999; Loisel et al. 2001, 2002, Mishonov et al. 2003; Stramska and Stramski 2005a, Gardner et al. 2006; Pabi and Arrigo 2006; Stramski et al. 2008; Son et al. 2009; Stramska 2009; Allison et al. 2010 a,

b; Duforêt-Gaurier et al. 2010, Van). These estimates were based on relatively short ocean color data sets (ten years or less), because longer time series were not available at the time. In this paper, the 16-year time series of POC concentrations derived from data collected by the Sea-viewing Wide Field-of-view Sensor (SeaWiFS) aboard the OrbView-2 satellite and the Moderate Resolution Imaging Spectroradiometer deployed on the Aqua (EOS PM satellite, MODIS-A) have been analyzed. These significantly longer data sets allow us to reevaluate the estimates of the POC reservoir in the global ocean more precisely and to investigate its variability and trends with higher confidence than it was done before.

## 2. Data and Methods

Methods used in this study are similar to those in Stramska (2014). Below we provide a brief overview of these methods.

The primary data set used in this study includes daily ocean surface POC concentrations derived from ocean color data collected by SeaWiFS and MODIS - Aqua. Each of these missions provided global coverage of remote sensing reflectances in selected spectral bands in the visible and near-infrared spectral regions at approximately every two days (e.g., Franz et al. 2007; Siegel et al., 2013). Data have been processed by NASA using standard procedures (O'Reilly et al. 1998; 2000; Franz et al. 2007). For our study we have downloaded Level 3 POC data (Standard Mapped Images, SMI) with a nominal 9.2 km resolution at the equator, reprocessing versions R2010.0 and R2013.1 of SeaWiFS and MODIS-A data, respectively. These POC estimates are based on the Stramski et al. (2008) algorithm.

We started our calculations with the highest possible resolution (daily fields of POC concentrations, in mg $m^{-3}$). Data processing steps included calculations of the 21-day moving averages to fill in the missing data. From these data we estimated the monthly, annual, and the 16-year averaged POC concentrations. To characterize six oceanic basins (North Atlantic, South Atlantic, North Pacific, South Pacific, Indian and Southern Oceans) regional averages were based on geographical boundaries defined in the International Hydrographic Organization document S-23 (IHO, 1953; Fourcy and Loverec, 2013). As in Stramska (2009), we have assumed that the North Atlantic and

North Pacific Oceans are limited by the 70°N latitude and that the Southern Ocean is located south from 50°S, which roughly corresponds to the Antarctic Convergence. Similar approach has been used before by Antoine at al., (1996) and Stramska (2009). The inland seas (e.g, Mediterranean, Black Sea, Baltic Sea, the Hudson Bay) have been excluded when regional averages for ocean basins have been calculated. Finally, data presented as regional averages (including time series plots) represent the weighted averages from all pixels within a given region. The weighted average accounts for the fact that pixel area at given latitude is equal to the cosine of this latitude multiplied by the pixel area at the equator (Campbell et al., 1995). In the final set, data in years 1998-2002 are from SeaWiFS, in 2003-2007 represent average daily POC concentrations from SeaWiFS and MODIS-A, while in 2008-2013 are from MODIS-A observations. Comparisons of the SeaWiFS and MODIS-A POC estimates in 2003-2007 showed a good agreement (e.g., see Stramska, 2014, Figure 2).

In addition to POC concentrations we have estimated POC reservoirs in the surface waters of the global ocean. Similarly to Stramska (2014), we have derived POC content of the oceanic euphotic depth ($z_{eu}$) and the mixed layer depth (MLD, see e.g., Niiler and Kraus 1977, Kraus et al. 1988, Lorbacher et al. 2006). The surface POC concentrations were converted to water column integrated POC biomass through the relationships derived from the Joint Global Ocean Flux Study experiment data (JGOFS, usjgofs.whoi.edu/jg/dir/jgofs/) (see Stramska, 2014 for details). To calculate POC biomass integrated over the mixed layer ($POC_{MLD}$) we have used the MLD estimates derived from ocean models (data available at web.science.oregonstate.edu/ocean.productivity/site.php, Behrenfeld et al. 2005, Westberry et al. 2008). These data have been provided at 8-day intervals, therefore we have carried out a linear interpolation to match the daily temporal resolution of the ocean color data. To calculate POC integrated over the euphotic depth ($POC_{Zeu}$) we have used the euphotic depth ($z_{eu}$) estimate provided by the NASA Ocean Color website (oceancolor.gsfc.nasa.gov) as the Zeu_Lee product (e.g., Lee et al. 2005a, b, 2007, Doron et al. 2007). Finally, we have derived estimates of the maximum POC ($POC_{max}$) content of the oceanic surface layer, using the greater of $POC_{MLD}$ or $POC_{Zeu}$ value at each pixel. To evaluate the sensitivity of our estimates to MLD estimates we have additionally used

mixed layer depth data from de Boyer Montégut (2004) made available by IFREMER/LOS Mixed Layer Depth Climatology website (www.ifremer.fr/cerweb/deboyer/mld). Other MLD data sets used for this purpose include data from the Argo Mixed Layers Project (Holte and Talley, 2009) at the Scripps Institution of Oceanography (http://mixedlayer.ucsd.edu) and from the Japan Argo Delayed-mode Data Base (Hosoda et al, 2010) (www.jamstec.go.jp/ARGO/argo_web/MILAGPV/index_e.html). We have also used data from the Global Ocean Data Assimilation System (GODAS) distributed by the US National Oceanic and Atmospheric Administration, Earth System Research Laboratory/Physical Sciences Division from their Web site at http://www.esrl.noaa.gov/psd/

To compare oceanic POC reservoirs and their variability with concurrent primary productivity (PP) estimates we have used data distributed through the Ocean Productivity Web Page (www.science.oregonstate.edu/ocean.productivity/) that include data from the Vertically Generalized Production Model, VGPM (Behrenfeld and Falkowski 1997), the Eppley-VGPM version of the model, and the Carbon-based Production Model, CBPM (Behrenfeld et al. 2005; Westberry et al. 2008).

To characterize the most important temporal scales of variability of POC, we performed time series analysis using algorithms described by Bendat and Piersol (2011). First, we subtracted off a linear trend, which was fitted to each time series record by a least square method. Next, the power spectra of the data series were obtained using a Fourier transform of the autocovariance function, to which Parzen weighting function was applied. In all cases considered here time series record consisted of a total number of N = 1024 data points, representing POC concentrations subsampled at 6 day time resolution form the original time series data. The autocovariance functions were calculated with the maximum time lag M = 150. The M value of 150 is a little beyond the value usually recommended (M = 0.1N), but this higher value of M increased the spectral resolution. Tests with gradually increasing the time lag from 100 to 150 indicated that the calculated spectra changed smoothly, and there were no spurious effects. Therefore, Figures included in the Results section are based on calculations with M = 150. The standard error is ~34% in the power spectral estimates. The multiyear trends for POC and

POC biomass presented in this study were derived using linear regression analysis (Bendat and Piersol, 2011)

Summarizing, in comparison to our earlier global POC estimates (e.g., Stramska, 2009), the estimates derived in the current paper are based on significantly longer data sets (16 years from 1998-2013). In addition, data employed in the current study originate from a more recent NASA reprocessing versions of the SeaWiFS and MODIS data sets (R2010.0 and R2013.1, respectively). Finally, the primary MLD data used in the current study is based on data-assimilating models tuned to the available in situ data (data from www.science.oregonstate.edu/ocean.productivity). In contrast, Stramska (2009) used MLD climatology data with monthly resolution (de Boyer Montegut et al., 2004). These data did not allow us to account for long term trends in the MLD.

## 3. Results

### 3.1 POC concentrations

Example 16-year averaged (1998-2013) monthly mean surface POC concentrations in the global ocean are presented in Figure 1 a and b. The main features on the maps are similar to POC distributions described before (e.g., Gardner et al., 2006. Stramska 2009; Duforêt-Gaurier et al., 2010). The major patterns of global POC concentration in the open ocean are oriented zonally. Generally, the highest values of surface POC concentration are observed in the summer of the northern hemisphere in the northern North Atlantic and in the Arctic regions (Figure 1 b). The lowest POC concentrations are present in the oligotrophic subtropical gyres, particularly in the South Pacific at 10-30$^{o}$S. Seasonal relocation of zonal patterns in maximum and minimum POC concentrations is also noticeable in Figure 1. For example, in the Atlantic and Pacific Oceans the minimum values of POC occur in the winter in the northern sections of the basins, while in the spring/summer they relocate south. The coefficient of variation (CV), defined as the ratio of standard deviation to the mean POC value at each pixel is shown in Figures 1 c and d for the months of February and July, respectively. The coefficient of variation indicates considerable interannual variability in regions with high phytoplankton productivity (i.e. North Atlantic, subarctic gyres, regions of coastal upwelling, SouthernOcean). For example, the coefficient of variation is around 50% in

the Northern Atlantic in July and in the Southern Ocean during austral summer CV also assumes high values in the regions of coastal upwelling and in some regions can be associated with variable position of major ocean currents.

The seasonal cycle is the most prominent characteristic feature of the variability of surface particulate organic matter concentration in the ocean (see also Loisel et al., 2002; Gardner et al., 2006, Duforêt-Gaurier et al., 2010; Vantrepotte and Mélin, 2011; Vantrepotte et al., 2011; Siegel et al., 2013). To better characterize seasonal cycle of POC we have plotted in Figure 2a time series of the surface POC concentrations averaged in different ocean basins. The problem of missing ocean color data is severe in the Southern Ocean during austral winter (this is noticeable in Figures 1 and 2a). The characteristic shapes in the time series of regional POC concentrations presented in Figure 2a are similar to those in Stramska (2009), but the interannual variability is more pronounced in the more recent data set. This can be partly explained by the fact that this new data set covers more years. In summary, the North Atlantic, North Pacific, and Southern Ocean waters are characterized by relatively high surface POC concentrations, while the South Pacific has the lowest 16-year average of POC concentration and the smallest amplitude of the annual cycle. The North Atlantic and North Pacific show particularly high POC concentrations during the northern hemisphere's spring and summer. The maximum daily 16-year regional average POC concentrations reaching ~110 mg $m^{-3}$ in the North Atlantic and ~80 mg $m^{-3}$ in the North Pacific are observed on year days 115-130. The average amplitude of the annual POC cycle is about 35 mg $m^{-3}$ and 30 mg $m^{-3}$ in the North Atlantic and North Pacific respectively. Similar amplitude for POC concentration averaged in the global ocean is only 10 mg $m^{-3}$. The annual cycle of surface POC concentration in the North Pacific and Indian Ocean includes additionally the second maximum occurring in the fall (~day 260-270). The maximum value of the globally averaged POC concentration is reached during northern hemisphere's late spring/early summer and again in the fall, while the minimum value is observed during the northern hemisphere's winter. The values of the 16-year average regional surface POC concentrations in each of the oceanic regions are compared in Table 1. Note that there is quite a good agreement between these estimates and those published in Stramska (2009).

The seasonal cycle of phytoplankton in many oceanic regions includes not only spring, but also fall phytoplankton blooms. It is natural to expect that this can have a significant influence on the variability patterns of POC. To investigate how significant is the relative contribution of variance at different time scales in comparison to the total variance in the times series, we have estimated power spectral density (Bendat and Piersol, 2011) of surface POC concentrations in regions where the time records of satellite observations have sufficiently good temporal resolution. Our results presented as power spectral density normalized to the total variance (see examples in Figure 2 b) indicate that there are three major types of the shape of the power spectra. In the first case, the POC variability is characterized by a prominent annual peak in the power spectrum, where almost all of the variance is concentrated. In the second case, the shape of the power spectrum is characterized by the presence of two statistically significant peaks, one in the annual and one in the semiannual period. The relative importance of these peaks can be different in different regions. Finally, in the third case, only the semiannual peak is statistically significant. To illustrate spatial variability of the relative importance of the annual and semiannual scales of variability we have divided the ocean into 5x5 degree boxes and estimated the power spectra of POC in each box (Figure 2c and d). The values of the normalized power spectral peaks in the annual and semiannual scales have been indicated by various colors. The results presented in Figure 2 c and d indicate that the annual peak usually assumes higher values than the semiannual peak. However, in some regions indicated by red/brown color in Figure 2 d coincident with blue color for the same geographical position in Figure 2 c, the semiannual peak is also significant. This can be observed for example, in the northern North Atlantic and Pacific, northern parts of the Arabian Sea and in the region of upwelling along the west coast of Africa. The presence of the semiannual peak is obviously associated with less variance attributed to the annual peak. An interesting study of the seasonal cycle of Chl and particulate matter in the ocean has been presented in Vantrepotte and Mélin (2011) and Vantrepotte et al. (2011). It seems that the main regions where the annual cycle has the strongest contribution to the total variance of POC in our Figure 2 are similar to the results for Chl presented in Figure 4 b in Vantrepotte and Mélin (2011). However it is quite difficult to make a more detailed comparison, because the calculation methods were

different in each study and for example it is not clear to us if the semiannual component of variability has been included in the seasonal cycle described by Vantrepotte and Mélin (2011) and Vantrepotte et al. (2011).

To better visualize the regional features of the annual POC cycle, we have plotted in Figure 3a and b maps of the annual minimum and maximum POC values at each pixel. Figures 3c and d provide information on when (day of the year) on average the POC concentrations assume minimum and maximum annual values. In addition, Figure 3e shows the amplitude of the annual cycle calculated as the difference between the maximum and the minimum POC concentration at each pixel. All data shown in Figure 3 are derived from the 16-year average daily time series of POC concentrations. The open ocean waters of the northern North Atlantic and northern North Pacific have the minimum and maximum POC values of about 60 mg $m^{-3}$ and 300 mg $m^{-3}$ respectively. The maximum POC concentrations observed in the oligotrophic gyres (20-30 mg $m^{-3}$) are lower than the minimum values in the northern North Atlantic and northern North Pacific. The most evident feature in Figure 3e is the high amplitude of the POC annual cycle in the northern North Atlantic and northern North Pacific waters. In the northern North Atlantic the amplitude of the annual POC cycle is about 160 mg $m^{-3}$ and more. In addition, quite high amplitude is also observed in the Southern Ocean. The lowest amplitude (10 mg $m^{-3}$) is detected in the region between $30^{o}$ N and $30^{o}$ S. It is also noticeable in Figure 3c and d that the timing of the annual maximum and minimum of the POC cycle is different in different regions. For example maximum POC concentrations are observed around day 90 at $30^{o}$N, around day 100 on $40^{o}$ N and around day 150 on $60^{o}$ N in the North Atlantic. This shift can be explained by the dependence of the POC concentration on the timing of the onset of the spring phytoplankton blooms, which are known to display similar time shifts (e.g., Martinez et al., 2011; Barton et al., 2015).

Apart from the seasonal cycle, there is also a significant interannual variability of POC concentration in the oceans. To investigate this variability we have plotted time series of the regionally averaged annual POC concentrations in Figure 4. A simple linear model for trend has been assumed, fitted by a least square method, and tested for statistical significance. This allowed us to quantify 16-year trends in POC concentrations summarized in Table 1. Statistically significant trends of decreasing surface POC

concentrations have been detected in the North Atlantic and North Pacific Oceans. In contrast, trends of increasing surface POC concentrations have been found in the South Pacific and in the Southern Ocean (Figure 4 d and f, Table1). Globally averaged annual surface ocean POC concentrations (Figure 4 e) do not show statistically significant trend in the 16-years considered. These results are consistent with Rousseaux and Gregg (2014) who have detected negative and positive trends in basin averaged surface chlorophyll concentrations in the northern and southern hemisphere, respectively. They have also concluded that the trend estimated for globally averaged Chl concentrations is not statistically significant. Phytoplankton biomass is a primary source for the POC matter in the ocean, therefore it seems that the long-term trends for POC and Chl should display similar tendencies. Since multiyear geophysical trends depend on the time period considered (due to climate related variability) it is important to note that Rousseaux and Gregg (2014) based their analysis on ocean color data from 1998-2012 (similar time period in comparison to our 1998-2013 data set).

### 3.2 POC reservoirs

As mentioned previously, one of our main goals is to reevaluate the POC reservoirs in the surface waters of the global ocean. In this section we describe the results of these calculations. We follow up the approach described in Stramska (2014) and base our estimates on the euphotic and the mixed layer depth concepts. In Figure 5 we have compared the 16-year averaged monthly $z_{eu}$ and MLD in February and July. Seasonal changes are noticeable on both the $z_{eu}$ and the MLD maps. In February (Figure 5a), the deepest euphotic zone occurs between 10 and 30$^{o}$ S. In July (Figure 5c) the deepest $z_{eu}$ is present between 10 and 30$^{o}$ N. The seasonal changes in the MLD are illustrated in Figures 5b and d (note the logarithmic scale). In the northern North Atlantic the MLD exceeds 300 m in February, but it shoals to about 20-40 m in July. In July the MLD reaches the greatest depth in the region between 50 and 60$^{o}$ S. The spatial MLD patterns shown in Figures 5b and d are similar to those shown in Stramska (2009), which were based on the MLD climatology derived from in situ observations (de Boyer Montégut et al., 2004). Note that often $z_{eu}$ and MLD show opposite patterns in their geographical distributions.

Maps of the water column integrated POC biomass derived using the $z_{eu}$ and MLD estimates are shown in Figure 6. These include the example estimates of the POC biomass integrated over the euphotic depth ($POC_{Zeu}$, Figure 6 a and b), over the MLD ($POC_{MLD}$, Figure 6c and d), and the $POC_{max}$ (Figure 6 e and f) taken as the greater of the $POC_{MLD}$ and $POC_{Zeu}$. Note that $POC_{Zeu}$ shows the smallest range of variability in comparison to the other POC biomass estimates. Low values of $POC_{Zeu}$ are observed zonally between 10 and 30° in the northern and in the southern hemispheres, with the lowest $POC_{Zeu}$ in the South Pacific (Fig 6a and b). The highest $POC_{Zeu}$ are noticeable in the equatorial zone and between 30 and 60° south and north. Seasonal variability is pronounced in the spatial patterns of $POC_{MLD}$ (Fig. 6c and d). The most striking observation is that regions of extremely high $POC_{MLD}$ are observed in February, north from $30^{o}$N. In July regions of extremely high $POC_{MLD}$ are present in the southern hemisphere, south from $30^{o}$S. Recall that the surface POC concentrations (Figure 1) have quite different seasonal patterns, that is POC concentrations in the northern North Atlantic and northern North Pacific are greater in July than in February. In comparison to $POC_{Zeu}$, the estimates of $POC_{MLD}$ show a much greater range of variability on a global scale and change from about 1g $m^{-2}$ in the oligotrophic gyres to about 20 g $m^{-2}$ in the eutrophic regions. There is also a seasonal shift in the location of the oligotrophic regions. The lowest $POC_{MLD}$ values occur at about 0-$30^{o}$S in February and at 10-$40^{o}$N in July. Understandably, patterns in $POC_{max}$ are similar to patterns in $POC_{MLD}$ in the higher latitudes and to $POC_{Zeu}$ in the regions located between $30^{o}$S and $30^{o}$N. Note that since $POC_{max}$ seems to be a more realistic estimate of POC reservoirs than $POC_{Zeu}$ or $POC_{MLD}$, most of our results presented below are focused on $POC_{max}$.

In Figure 7 the 16-year averaged annual cycles of regional $POC_{max}$ are illustrated. These results can be compared with Figure 2, where we presented similar plots for POC concentrations. The most obvious difference between time series shown in Figure 2 and 7 is the timing of the maximum. The maximum in $POC_{max}$ series in the North Atlantic and North Pacific is observed earlier in the year than the annual maximum in the POC concentration (days 65-96 for $POC_{max}$ and days 115-130 for POC). The fall POC concentration maximum in the North Pacific does not translate to a significant maximum in $POC_{max}$. In the South Atlantic, the maximum in the time series of $POC_{max}$ is observed

later in the year than the maximum in the POC time series. In the Indian and South Pacific Oceans the fall maxima in POC concentration correspond to well pronounced maxima in $POC_{max}$. Thus, it becomes evident that surface POC concentrations alone do not allow us to trace the variability in POC reservoirs, if we do not combine them with additional information about the variability of the MLD and $z_{eu}$.

The characteristic features of the average annual cycle of $POC_{max}$ are also presented in Figure 8 as maps of the annual minimum and maximum $POC_{max}$ values (Figure 8 a and b), the timing (day of the year) when they are observed (Figure 8 c and d), and the amplitude of the annual cycle (Figure 8 e). The highest maximum $POC_{max}$ values are observed in the northern North Atlantic and in the Southern Ocean, while the lowest ones occur in the zone between $30^oS$ and $30^oN$. The highest annual amplitude evident in the northern North Atlantic is as high as 30 g $m^{-2}$. There is an abrupt change in the timing of the annual maximum and minimum in $POC_{max}$ between the northern and the southern hemispheres. This is also evident in Figure 9 a, where we compared the timing of the annual maximum in POC and $POC_{max}$. The data shown in Figure 9a are based on the 16-year averaged daily POC and $POC_{max}$ values averaged into latitudinal zones (1 degree wide) in the Atlantic Ocean. The differences in the timing of maximum in the average annual cycles of POC and $POC_{max}$ are more pronounced in the regions located north from the $40^oN$ and south from $40^oS$. For example, in the north the maximum of POC concentration is observed later in the year than the maximum in the $POC_{max}$ cycle. This is linked to a well-pronounced annual cycle of the MLD in these regions. Example annual cycles of $POC_{max}$, POC, PP, and MLD for a selected open ocean region in the northern North Atlantic (located between 60-46.7$^o$ N and 47-15$^o$ W) are compared in Figure 9 b and c. As can be seen in Figure 9b the maximum in $POC_{max}$ in this region occurs when the MLD is still deep, but starts its seasonal decrease. In contrast the maxima in POC concentration and PP are observed later in the year, when the MLD reaches its minimum. This can be explained by the fact that when the MLD shoals part of the POC biomass (included in the $POC_{max}$ estimate when the MLD was deeper) becomes excluded from the MLD based estimates. Thus, at the time when MLD undergoes significant seasonal shoaling there is a considerable loss of POC biomass incorporated in the water column integrated POC estimate. In contrast, because the water column mixing

becomes less intense when the MLD decreases, the losses of POC particles from ocean surface to greater depths due to mixing become smaller. This is why we observe increase in the surface POC concentration at this time. This increase is partly due to the fact that there is also a seasonal increase of PP, which is the source of new POC particles in the surface waters.

To investigate inter-annual variability in $POC_{max}$ we have plotted in Figure 10 time series of the regional annual averages of $POC_{max}$. This Figure is similar to Figure 4 where inter-annual variability in regionally averaged surface POC concentrations was discussed. The data shown in Figure 10 and the summary of the statistical analysis presented in Table 2 indicate that except for the North Pacific, all of the regionally averaged $POC_{max}$ estimates show statistically significant trends of increasing $POC_{max}$ in the 16 years of ocean color observations. Trend is strongest for the Southern Ocean. Trend is also significant for the global estimates. Previous analyses of the POC reservoirs based on satellite data (e.g., Stramska, 2009; Allison et al., 2010a, b; Duforêt-Gaurier et al. 2010) did not report such trends, probably because data sets at that time were too short to show evidence of multi-year trends.

More insight into the global distribution of trends can be gained by inspecting Figure 11, where we have plotted several maps. These maps have been created in order to identify the geographical locations where trends are well pronounced. Trends are indicated by colors only for the pixels with statistically significant trends. One has to be aware of the fact that the results presented in this way are sensitive, for example, to variable locations of fronts and eddies, while the regional trends presented in Figure 10 are not. Figure 11 a indicates regions where trends in surface POC concentrations are positive (yellow and red pixels) and negative (blue pixels). As we can see the decrease of POC concentration has been mostly observed in the northern hemisphere, while the increase is mostly attributed to the waters located south from $30^{o}$S. The geographical patterns in POC trends are similar to patterns in Chl trends in Figure 6 in Rousseaux and Gregg (2014). Trends in the $POC_{Zeu}$, $POC_{MLD}$ and $POC_{max}$ are summarized in Figures 11b, c, and d. Now the regions with negative trends (blue pixels) are mostly confined to a limited area of the northern North Atlantic and Pacific (north from 50-$60^{o}$N). In most cases when the trend is significant it has positive values. The strongest positive trend in

$POC_{max}$ has been observed in the Southern Ocean. Positive trends in the $POC_{Zeu}$, $POC_{MLD}$ and $POC_{max}$ are in most regions associated with positive trends in $z_{eu}$ and/or MLD (Figure 11e and f). In the Southern Ocean $POC_{Zeu}$ shows a positive trend even if $z_{eu}$ has a negative trend.

It is interesting to compare trends in the water column integrated POC biomass with trends in the primary production, PP (Figure 12). We have calculated trends in PP estimates taken from the Ocean Productivity Web Page (www.science.oregonstate.edu/ocean.productivity/) based on three ocean color PP models: the Vertically Generalized Production Model (VGPM, Behrenfeld and Falkowski 1997), the Eppley-VGPM version of the model, and the Carbon-based Production Model (CBPM, Behrenfeld et al. 2005, Westberry et al. 2008). All three models indicate that there is a negative trend in PP in most of the oceanic regions. The negative trend is most pronounced in the data based on the CBPM model. The trends in the VGPM and Eppley models are similar, therefore in Figure 12a and b we have only plotted the results from the VGPM and CBPM models. Negative trends in the estimates of oceanic PP have been reported before (Behrenfeld et al., 2006; Rousseaux and Gregg, 2014). Using the PP estimates we have also estimated the ratio of the 16-year average daily PP to the 16-year average $POC_{max}$. The maps of PP/ $POC_{max}$ based on VGPM and CBPM models are displayed in Figure 12c and d respectively. These results indicate that the highest $PP/POC_{max}$ ratio of about 0.1- 0.2 occurs in the region located between $30^{o}$S and $30^{o}$N. The lowest $PP/POC_{max}$ ratio is about an order of magnitude smaller (0.02) and is observed in the Southern Ocean as well as in the northern North Atlantic. Because the trend in PP is mostly negative and the trend in the $POC_{max}$ is in most regions positive, trend in the $PP/POC_{max}$ ratio is almost everywhere negative. This suggests that the POC particles tend to have longer residence time in the surface waters (since we observe that PP is decreasing but $POC_{max}$ is increasing). Increase in the POC residence time could be related to slower transport of particles to deeper water layers or slower recycling in the surface waters. At present it is impossible to fully explain the findings described above. Our results underline the importance of future efforts to collect extensive in situ data sets complemented by modeling studies in order to develop an in-depth understanding of the ecological interactions responsible for the observed trends. It is also possible that longer

ocean color time series available in the future will change our perception of these trends. As discussed by Henson et al. (2010), longer time series of ocean color data are needed to fully explain whether trends detected in the current ocean color data sets are related to interannual fluctuations or if they are an expression of the long-term trends linked to climate change.

## 4. Discussion and Conclusions

Our calculations include some assumptions. First, time series analyzed in this paper were collected by two ocean color satellites. Even if the NASA Ocean Biology Processing Group (OBPG) continuously incorporates new knowledge of sensor-specific instrument calibrations and validations, there is some bias between the radiometric data sets (http://oceancolor.gsfc.nasa.gov/ANALYSIS/PROCTEST/). To evaluate if this bias can significantly influence our results we have compared SeaWiFS and MODIS POC concentrations from years 2003-2007, when reliable ocean color data were available from both SeaWiFS and MODIS radiometers. This comparison showed that in the open ocean waters (waters with depth greater than 200 m) POC concentrations derived from MODIS are smaller than the POC concentrations derived from SeaWiFS on average by about 0.15 $mg/m^2$. Our test calculations indicated that when we applied a simple correction for this bias, the globally averaged 16-year trend for POC concentration would still be statistically not significant and the patterns in regional trends would remain similar to those described in the results section. We have also detected similar patterns in regional trends of POC concentration when we only used MODIS data from 2003-2014 in the calculations. The correction for bias would slightly increase the global trend in POC reservoirs.

Another assumption is that potentially larger errors in POC retrievals in coastal waters with algorithms developed for open ocean applications (Stramski et al., 2008) do not significantly influence our main results. To verify this assumption we have carried out additional calculations, which indicated that if we doubled POC concentrations in coastal regions (where water depth is 200 m or less), the globally averaged POC concentrations would increase by less than 6 %. On the other hand if POC concentrations in coastal regions in our original estimates were overestimated by 100%, the globally

averaged POC concentrations could have been overestimated by about 3 %. Note that these potential errors in coastal POC retrievals would not influence the results for the open ocean pixels presented in the maps.

We have based our calculations on MLD data sets used by Behrenfeld et al. (2005, 2006), to be consistent with their PP estimates used in our study (PP has been derived using the same MLD data set). To estimate the sensitivity of our results to MLD we have carried out additional calculations. In these calculations we have used MLD data sets based on re-analysis of in situ data from research vessels, moorings and drifters (de Boyer Montégut et al. 2004) and newer data sets based on measurements from Argo floats (Holte and Talley, 2009; Hosoda et al., 2010). In addition to in situ data, MLD estimates can be based on numerical models that assimilate oceanographic data. In other words, in situ oceanographic data can be reanalyzed through data assimilative models to provide information about MLD on a regular spatial grid. One example of such data set (Behrenfeld et al. 2005, 2006; Westberry et al., 2008) has been used in our original calculations. Another similar MLD data set is available from the NCEP reanalysis. The results from calculations with different MLD data sets summarized in Table 3 indicate that globally averaged $POC_{mld}$ estimate would change by up to +/- 16% depending on what MLD data are used. Note that all the MLD data sets used for the sensitivity tests have lower temporal (monthly) and spatial resolution (depends on the data set) than the data used in our core calculations.

The monthly NCEP MLD data support an important aspect of our original analysis, the observation that MLD has most likely been deepening in some oceanic regions during the last 16 years. Increasing mixed layer depths have been also reported in previous analysis of archive Argo profiles published by Carton et al. (2008). The authors found that at decadal periods the winter–spring mixed layers of the North Atlantic and North Pacific were deepening by 10–40 m over the 45-yr period (1960–2004). The long-term mixed layer deepening was even stronger (50–100 m) in the North Atlantic subpolar gyre. This supports the tendencies derived from analysis of our primary data set.

Summarizing, our analysis of 16-year time series of POC concentrations indicate that the range of global and regional average surface concentrations are similar to those

derived earlier with the 10-year long time series data (Stramska, 2009). Surface POC concentrations undergo considerable seasonal variability. The annual amplitude of the annual cycle as well as the maximum and minimum annual POC concentrations depend strongly on the geographical location. We have also shown that the POC concentrations in the last 16 years (1998-2013) have been decreasing in the North Atlantic and North Pacific, increasing in the South Pacific and the Southern Ocean, while the trends are not statistically significant in the South Atlantic and Indian Oceans, as well as for the globally averaged concentrations.

We have estimated POC biomass integrated in the water column over the euphotic and mixed layer depths. The results from these calculations show that the global estimate of POC reservoir is larger if the POC biomass estimate is based on the MLD than if it is based on the $z_{eu}$. However we suggest that the more realistic is the estimate that for each geographical location (each pixel of the ocean color data) assumes that the depths of the surface layer should be represented by the greater of the MLD or $z_{eu}$. Similar assumption has been used to estimate the global ocean PP (Behrenfeld et al., 2013). Using this assumption we have shown that the average POC biomass in the surface waters of the global ocean is on the order of 5 g $m^{-2}$. Note that this estimate agrees well with our earlier estimate of POC biomass based on slightly different assumptions and shorter ocean color data time series (Stramska, 2009) and with estimates published by other authors (e.g., Gardner et al., 2006; Duforêt-Gaurier et al., 2010).

We have shown that similarly to surface POC concentration, the water column integrated biomass $POC_{max}$ also undergoes an annual cycle. There are however significant differences between the annual cycles of POC concentration and $POC_{max}$. First, the size of the annual amplitude in comparison to the global average value is significantly larger for the $POC_{max}$ ($POC_{max}$ amplitude in the northern North Atlantic is about 6 times the global average $POC_{max}$) than for the POC time series (POC amplitude in the northern North Atlantic is about 4.4 times the global average concentration). The geographical patterns in the global POC and $POC_{max}$ distributions are different. A noticeable difference is that the relative importance of the POC reservoir in the Southern Ocean is more pronounced on the $POC_{max}$ maps than the POC concentration, because the MLD is deep in this region. Finally, the timing of the maximum POC concentration can

be significantly shifted in comparison to the timing of the maximum in $POC_{max}$ annual cycle. This is especially evident in the temperate and high latitude regions. All these results underline the fact that we cannot interpret directly spatial and temporal variability in the distributions of the ocean surface POC concentrations as the variability in the POC biomass in the ocean. Such interpretation requires parallel knowledge about surface column water structure, or at least the information about the MLD and $z_{eu}$.

Our analysis indicates that long-term trends in POC concentration and POC biomass are statistically significant in many regions. These results should be treated with caution, as the presently available data sets are still too short to develop a full understanding of climate related trends (e.g., Henson et al., 2010). Nevertheless our calculations have shown that the regional trends in surface POC concentrations can disagree with trends in the water column integrated POC biomass. The reason for this is that estimates of POC biomass depend on the estimates of MLD and $z_{eu}$. Our results suggest that in the last 16-years we have experienced global trend of increasing average water column integrated POC biomass. This result is due to a combined effect of increasing surface POC concentrations (mainly in the southern hemisphere) as well as the trend of increasing $z_{eu}$ and MLD in some ocean basins. However it is somewhat startling that the increase in the POC biomass is observed while at the same time ocean color data indicate a decrease in the global oceanic PP. This would suggest that the ratio of PP/ $POC_{max}$ is decreasing almost everywhere in the ocean (Figure 12). At present it is difficult to fully explain this observation, but such a decrease could indicate that the biological pump in the ocean is weakening. In general, it is possible that POC particles are increasing their residence time in the surface waters due to changes in physical and/or biological processes. For example, the mixing events in surface waters can be less efficient in transporting the particles to subsurface waters (Stramska, 2010), or there are shifts in the functional types of phytoplankton and ecosystem structure and their interactions (Siegel et al., 2014). It is also possible, that there are some systematic errors in our estimates of $POC_{max}$ and/or PP. Longer time series of consistent ocean color data supported by special in situ experiments and modeling efforts are needed to fully investigate these issues.

**Acknowledgments**. Financial support for this research was provided by the National Science Centre (NCN) in Poland through grant 2011/01/M/ST10/07728 „ Global estimates of particulate organic carbon reservoir and export flux in the ocean based on satellite ocean color data“. Partial support for MS comes also from the statutory funds of the Institute of Oceanology of the Polish Academy of Sciences (IO PAN). The authors are grateful to all the persons involved in the programs providing free access to the data sets used in this study. The ocean color data were made available through the NASA Ocean Color Web (oceancolor.gsfc.nasa.gov/). The Ocean Productivity Web at the Oregon State University (www.science.oregonstate.edu/ocean.productivity/) supplied primary productivity and mixed layer depth data. We are also grateful for mixed layer depth data made available by IFREMER/LOS Mixed Layer Depth Climatology website (www.ifremer.fr/cerweb/deboyer/mld), Argo Mixed Layers Project at the Scripps Institution of Oceanography (http://mixedlayer.ucsd.edu), and the Japan Argo Delayed-mode Data Base (www.jamstec.go.jp/ARGO/argo_web/MILAGPV/index_e.html). Global Ocean Data Assimilation System (GODAS) data were provided by the US National Oceanic and Atmospheric Administration, Earth System Research Laboratory/Physical Sciences Division from their Web site at http://www.esrl.noaa.gov/psd/ We would also like to thank Sebastian Meler from the IO PAN for help with data transfers.

Table 1. Global and regional estimates of the 16-year average POC concentration (in mg $m^{-3}$) and 16-year trends ($p<0.05$, 95% confidence level).

| Region | POC mg $m^{-3}$ | Trend mg $m^{-3}y^{-1}$ | R |
|---|---|---|---|
| Global | 67.7 | not significant | - |
| N. Atlantic | 86.8 | -0.42 | 0.63 |
| S. Atlantic | 73.9 | not significant | - |
| N. Pacific | 63.3 | -0.25 | 0.58 |
| S. Pacific | 47.8 | +0.13 | 0.54 |
| Indian | 60.7 | not significant | - |
| S. Ocean | 70.1 | +1.20 | 0.70 |

Table 2. Global and regional estimates of the average POC biomass (in g $m^{-2}$) integrated down to the euphotic depth ($POC_{Zeu}$), mixed layer depth ($POC_{MLD}$), and $POC_{max}$, and 16-year statistically significant trends ($p<0.05$, 95% confidence level) in $POC_{max}$.

| Region | $POC_{Zeu}$ g $m^{-2}$ | $POC_{MLD}$ g $m^{-2}$ | $POC_{max}$ g $m^{-2}$ | $POC_{max}$ trend mg $m^{-2}y^{-1}$ | R |
|---|---|---|---|---|---|
| Global | 3.97 | 3.92 | 5.03 | 25.74 | 0.61 |
| N. Atlantic | 4.30 | 4.43 | 5.77 | 18.34 | 0.45 |
| S. Atlantic | 4.09 | 3.99 | 5.26 | 26.41 | 0.49 |
| N. Pacific | 3.96 | 2.98 | 4.55 | not significant | |
| S. Pacific | 3.63 | 2.87 | 4.22 | 15.70 | 0.65 |
| Indian | 3.99 | 3.82 | 5.22 | 27.10 | 0.54 |
| S. Ocean | 3.80 | 6.48 | 7.84 | 241.51 | 0.83 |

Table 3. Difference in % between the 16-year averaged $POC_{MLD\_1}$ estimate derived using the MLD data from the Ocean Productivity Web (www.science.oregonstate.edu/ocean.productivity/) and $POC_{MLD\_x}$ estimates based on other MLD data sets. Symbol $\sigma_\theta$ indicates potential density. In each case the difference has been calculated as $100\%*(POC_{MLD\_1} - POC_{MLD\_x})/POC_{MLD\_1}$. The $POC_{MLD\_1}$ and $POC_{MLD\_x}$ have been averaged in the region between $65^oN - 65^oS$, because Argo based MLD climatology does not have sufficient coverage in the polar regions. The SIO data (Holte and Talley, 2009) are from the Argo Mixed Layers Project (http://mixedlayer.ucsd.edu), the Jamstec data (Hosoda et al., 2010) are from the Japan Argo Delayed-mode Data Base (www.jamstec.go.jp/ARGO/argo_web/MILAGPV/index_e.html), the IFREMER data (de Boyer Montégut et al., 2004) have been downloaded from (www.ifremer.fr/cerweb/deboyer/mld), and the NCEP GODAS data come from http://www.esrl.noaa.gov/psd/.

| MLD data set | MLD algorithm | Difference (%) |
|---|---|---|
| SIO | density algorithm | 16.3 |
| SIO | density threshold | 10.7 |
| SIO | temperature algorithm | 11.6 |
| SIO | temperature threshold | 5.5 |
| Jamstec | shallower thickness, either $\Delta\sigma_\theta$=0.03kg/m$^3$ or $\Delta$T=0.2°C | -7.7 |
| Ifremer | MLD_DT02 = depth where (T = $T_{10m}$ ± 0.2 °C) | 13.1 |
| Ifremer | fixed density threshold criterion (0.03kg/m$^3$) | 11.3 |
| Ifremer | variable threshold criterion (equivalent to a 0.2°C decrease) | 14.8 |
| NCEP | from data assimilative ocean model | -15.8 |

**References**

Antoine, D., Andre,J.-M., Morel,A., 1996. "Oceanic Primary Production 2. Estimation at Global Scale from Satellite (Coastal Zone Color Scanner) Chlorophyll." *Global Biogeochemical Cycles* 10, 57–69.

Allison, D. B., D. Stramski, and B. G. Mitchell. 2010a. "Empirical Ocean Color Algorithms for Estimating Particulate Organic Carbon in the Southern Ocean." *Journal of Geophysical Research* 115: C10044. doi:10.1029/2009JC006040.

Allison, D. B., D. Stramski, and B. G. Mitchell. 2010b. "Seasonal and Interannual Variability of Particulate Organic Carbon within the Southern Ocean from Satellite Ocean Color Observations." *Journal of Geophysical Research* 115: C06002. doi:10.1029/2009JC005347.

Barton, A. D., Lozier, M. S. and Williams, R. G. 2015. "Physical controls of variability in North Atlantic phytoplankton communities." *Limnology and Oceanography* 60, 181–197. doi: 10.1002/lno.10011

Behrenfeld, M.J. S.C. Doney, I. Lima, E.S. Boss, D.A. Siegel, 2013. "Annual Cycles of Ecological Disturbance and Recovery Underlying the Subarctic Atlantic Spring Plankton Bloom." *Global Biogeochemical Cycles*, 27, DOI: 10.1002/gbc.20050

Behrenfeld, M.J., O'Malley, R.T., Siegel, D.A., McClain, C.R., Sarmiento, J.L., Feldman, G.C., Milligan, A.J., Falkowski, P.G., Letelier, R.M., Boss, E.S. 2006. "Climate-Driven Trends in Contemporary Ocean Productivity." *Nature* , 444, 752–755.

Behrenfeld, M. J., E. Boss, D. A. Siegel, and D. M. Shea. 2005. "Carbon-based Ocean Productivity and Phytoplankton Physiology from Space." *Global Biogeochemical Cycles* 19: GB1006. doi:10.1029/2004GB002299.

Behrenfeld, M. J., and P. G. Falkowski. 1997. "Photosynthetic Rates Derived from Satellite-Based Chlorophyll Concentration." *Limnology and Oceanography* 42: 1–20. doi:10.4319/lo.1997.42.1.0001.

Bendat, J.S., Piersol, A.G., 2011. Random Data: Analysis and Measurement Procedures. In: Wiley Series in Probability and Statistics. Wiley, p. 640.

Campbell, J. W., J. M. Blaisdell, and M. Darzi. 1995. "Level-3 SeaWiFS Data Products: Spatial and Temporal Binning Algorithms." SeaWiFS Technical Report Series 32: 73.

Carton, J.A., S.A. Grodsky, and H. Liu, 2008. Variability of the oceanic mixed layer 1960-2004, J. Clim., 21,1029-1047.

de Boyer Montégut, C., G. Madec, A. S. Fischer, A. Lazar, and D. Iudicone. 2004. "Mixed Layer Depth over the Global Ocean: an Examination of Profile Data and a

Profile-Based Climatology." *Journal of Geophysical Research* 109, C12003. doi:10.1029/2004JC002378,

Doron, M., M. Babin, A. Mangin, and O. Hembise. 2007. "Estimation of Light Penetration, and Horizontal and Vertical Visibility in Oceanic and Coastal Waters from Surface Reflectance." *Journal of Geophysical Research* 112: C06003. doi:10.1029/2006JC004007.

Duforêt-Gaurier, L., H. Loisel, D. Dessailly, K. Nordkvist, and S. Alvain. 2010. "Estimates of Particulate Organic Carbon over the Euphotic Depth from In Situ Measurements. Application to Satellite Data over the Global Ocean." *Deep Sea Research Part I: Oceanographic Research Papers* 57: 351–367. doi:10.1016/j.dsr.2009.12.007.

Dunne, J., Sarmiento, J.L., Gnanadesikan, A. 2007. "A Synthesis of Global Particle Export from the Surface Ocean and Cycling through Ocean Interior and Seafloor. *Global Biogeochemical Cycles* 21, doi:10.1029/2006GB002907.

Fourcy, D. and Lorvelec, O., 2013. "A New Digital Map of Limits of Oceans and Seas Consistent with High-Resolution Global Shorelines." *Journal of Coastal Research*, 29(2), 471-477. doi:10.2112/JCOASTRES-D-12-00079.1

Franz, B. A., S. W. Bailey, P. J. Werdell, and C. R. McClain. 2007. "Sensor-Independent Approach to the Vicarious Calibration of Satellite Ocean Color Radiometry." *Applied Optics* 46: 5068– 5082. doi:10.1364/AO.46.005068.

Gardner, W. D., A. V. Mishonov, and M. J. Richardson. 2006. "Global POC Concentrations from In-Situ and Satellite Data." *Deep Sea Research Part II: Topical Studies in Oceanography* 53: 718–740. doi:10.1016/j.dsr2.2006.01.029.

Henson, S. A., J. L. Sarmiento, J. P. Dunne, L. Bopp, I. Lima, S. C. Doney, J. John, and C. Beaulieu. 2010. "Detection of Anthropogenic Climate Change in Satellite Records of Ocean Chlorophyll and Productivity." *Biogeosciences* 7, 621–640. doi:10.5194/bg-7-621-2010.

Holte J., and L. Talley. 2009. "A New Algorithm for Finding Mixed Layer Depths with Applications to Argo Data and Subantarctic Mode Water Formation". *Journal of Atmospheric and Oceanic Technology*, 26, 1920–1939.doi: http://dx.doi.org/10.1175/2009JTECHO543.1

Honjo, S., Manganini, S.J., Krishfield, R.A., Francois, R., 2008. "Particulate Organic Carbon Fluxes to the Ocean Interior and Factors Controlling the Biological Pump: a Synthesis of Global Sediment Trap Programs Since 1983." *Progress in Oceanography* 76, 217–285.

Hosoda, S., T. Ohira, K. Sato, and T. Suga, 2010. "Improved description of global mixed-layer depth using Argo profiling floats." *Journal of Oceanography*, 66, 2010,773-787.

IPCC, 2007, In: Solomon, S., Qin, D., Manning, M., et al. (Eds.), Climate Change 2007: the Physical Science Basis. Contribution of Working Group 1 to the Fourth Assessment Report of the Intergovernmental Panel on Climate Change. Intergovernmental Panel on Climate Change, Cambridge/New York.

IHO, 1953. "Limits of Oceans and Seas", 3rd edition. Special Publication No. 23 (S-23). Monaco: International Hydrographic Organization.

Kraus, E. B., R. Bleck, and H. P. Hanson. 1988. "The Inclusion of a Surface Mixed Layer in a Large-scale Circulation Model." In Small Scale Turbulence and Mixing in the Ocean, edited by J. C. J. Nihoul and B. M. Jamart, 51–62. Amsterdam: Elsevier.

Laws, E. A., P. G. Falkowski, W. O. Smith, H. Ducklow, and J. J. McCarthy. 2000. "Temperature Effects on Export Production in the Open Ocean." *Global Biogeochemical Cycles* 14: 1231–1246. doi:10.1029/1999GB001229.

Lee, Z.-P., M. Darecki, K. L. Carder, C. O. Davis, D. Stramski, and W. J. Rhea. 2005a. "Diffuse Attenuation Coefficient of Downwelling Irradiance: An Evaluation of Remote Sensing Methods." *Journal of Geophysical Research* 110: C02017. doi:10.1029/2004JC002573.

Lee, Z.-P., K. P. Du, and R. Arnone. 2005b. "A Model for the Diffuse Attenuation Coefficient of Downwelling Irradiance." *Journal of Geophysical Research* 110: C02016. doi:10.1029/2004JC002275.

Lee, Z.-P., A. Weidemann, J. Kindle, R. Arnone, K. L. Carder, and C. Davis. 2007. "Euphotic Zone Depth: Its Derivation and Implication to Ocean-Color Remote Sensing." *Journal of Geophysical Research* 112: C03009. doi:10.1029/2006JC003802.

Loisel, H., E. Bosc, D. Stramski, K. Oubelkheir, and P.-Y. Deschamps. 2001. "Seasonal Variability of the Backscattering Coefficient in the Mediterranean Sea Based on Satellite SeaWiFS Imagery." *Geophysical Research Letters* 28: 4203–4206. doi:10.1029/2001GL013863.

Loisel, H., J.-M. Nicolas, P.-Y. Deschapms, and R. Frouin. 2002. "Seasonal and Inter-Annual Variability of Particulate Organic Matter in the Global Ocean." *Geophysical Research Letters* 29 (24): 2196. doi:10.1029/2002GL015948.

Longhurst, A. R., and W. G. Harrison. 1989. "The Biological Pump: Profiles of Plankton Production and Consumption in the Upper Ocean." *Progress in Oceanography* 22: 47–123. doi:10.1016/ 0079-6611(89)90010-4.

Lorbacher, K., D. Dommenget, P. P. Niiler, and A. Köhl. 2006. "Ocean Mixed Layer Depth: A Subsurface Proxy of Ocean-Atmosphere Variability." *Journal of Geophysical Research* 111: C07010. doi:10.1029/2003JC002157.

Martinez, E., D. Antoine, F. D'Ortenzio, and C. de Boyer Montégut. 2011. "Phytoplankton spring and fall blooms in the North Atlantic in the 1980s and 2000s." Journal of Geophysical Research 116, doi:10.1029/2010JC006836.

Mishonov, A. V., W. D. Gardner, and M. J. Richardson. 2003. "Remote Sensing and Surface POC Concentration in the South Atlantic." *Deep Sea Research Part II: Topical Studies in Oceanography* 50: 2997–3015. doi:10.1016/j.dsr2.2003.07.007.

Niiler, P. P., and E. B. Kraus. 1977. "One-dimensional Models of the Upper Ocean." In Modelling and Predictions of the Upper Layers of the Ocean, edited by E. B. Kraus, 143–172. Oxford: Pergamon.

O'Reilly, J. E., S. Maritorena, B. G. Mitchell, D. A. Siegel, K. L. Carder, S. A. Garver, M. Kahru, and C. R. McClain. 1998. "Ocean Color Chlorophyll Algorithms for SeaWiFS." *Journal of Geophysical Research* 103: 24937–24953. doi:10.1029/98JC02160.

O'Reilly, J. E., S. Maritorena, D. A. Siegel, M. C. O'Brien, D. Toole, B. G. Mitchell, and M. Kahru et al. 2000. "Ocean Color Chlorophyll a Algorithms for SeaWiFS, OC2 and OC4: Version 4." NASA Technical Memo, 2000-206892 11: 9–27.

Pabi, S., and K. R. Arrigo. 2006. "Satellite Estimation of Marine Particulate Carbon in Waters Dominated by Different Phytoplankton Taxa." *Journal of Geophysical Research* 110: C10018. doi:10.1029/2005JC003137.

Rousseaux, C.S., Gregg, W.W., 2014. "Interannual Variation in Phytoplankton Primary Production at A Global Scale." *Remote Sensing* 6, 1-19. doi:10.3390/rs6010001

Siegel, D. A., M. J. Behrenfeld, S. Maritorena, C. R. McClain, D. Antoine, S. W. Bailey, P. S. Bontempi, E. S. Boss, H. M. Dierssen, S. C. Doney, R. E. Eplee, R. H. Evans, G. C. Feldman, E. Fields, B. A. Franz, N. A. Kuring, C. Mengelt, N. B. Nelson, F. S. Patt, W. D. Robinson, J. L. Sarmiento, C. M. Swan, P. J. Werdell, T. K. Westberry, J. G. Wilding, and J. A. Yoder. 2013. "Regional to Global Assessments of Phytoplankton Dynamics from the SeaWiFS Mission." *Remote Sensing of Environment* 135: 77–91. doi:10.1016/j.rse.2013.03.025.

Siegel, D. A., K. O. Buesseler, S. C. Doney, S. F. Sailley, M. J. Behrenfeld, and P. W. Boyd 2014. "Global Assessment of Ocean Carbon Export by Combining Satellite Observations and Food-Web Models". *Global Biogeochemical Cycles*, 28, 181–196, doi:10.1002/2013GB004743.

Son, Y. B., W. D. Gardner, A. V. Mishonov, and M. J. Richardson. 2009. "Multispectral Remote Sensing Algorithms for Particulate Organic Carbon (POC): The Gulf of Mexico." *Remote Sensing of Environment* 113: 50–61. doi:10.1016/j.rse.2008.08.011.

Stramska, M., 2014. “Particulate Organic Carbon in the Surface Waters of the North Atlantic: Spatial and Temporal Variability Based on Satellite Ocean Colour.” *International Journal of Remote Sensing* 35: 4717–4738, http://dx.doi.org/10.1080/01431161.2014.919686

Stramska, M. 2009. “Particulate Organic Carbon in the Global Ocean Derived from SeaWiFS Ocean Color.” *Deep Sea Research I*. doi:10.1016/j.dsr.2009.04.009

Stramska, M., and D. Stramski. 2005a. “Variability of Particulate Organic Carbon Concentration in the North Polar Atlantic Based on Ocean Color Observations with Sea-viewing Wide Field-of view Sensor (SeaWiFS).” *Journal of Geophysical Research* 110: C10018. doi:10.1029/2004JC002762.

Stramska, M., and D. Stramski. 2005b. “Effects of a Nonuniform Vertical Profile of Chlorophyll Concentration on Remote-Sensing Reflectance of the Ocean.” *Applied Optics* 44: 1735–1747.doi:10.1364/AO.44.001735.

Stramski, D., R. A. Reynolds, M. Babin, S. Kaczmarek, M. R. Lewis, R. Röttgers, A. Sciandra, M. Stramska, M. S. Twardowski, B. A. Franz, and H. Claustre. 2008. “Relationships between the Surface Concentration of Particulate Organic Carbon and Optical Properties in the Eastern South Pacific and Eastern Atlantic Oceans.” *Biogeosciences* 5: 171–201.
doi:10.5194/bg-5-171-2008. www.biogeosciences.net/5/171/2008/.

Stramski, D., R. A. Reynolds, M. Kahru, and B. G. Mitchell. 1999. “Estimation of ParticulateOrganic Carbon in the Ocean from Satellite Remote Sensing.” *Science* 285: 239–242. doi:10.1126/science.285.5425.239.

Vantrepotte V., Mélin, F. 2011. “Inter-annual variations in the SeaWiFS global chlorophyll a concentration (1997-2007).” Deep Sea Research I, doi:10.1016/j.dsr.2011.02.003.

Vantrepotte V., Loisel H., Mélin F., Desailly D. ,Duforêt-Gaurier L. 2011. “Global particulate matter pool temporal variability over the SeaWiFS period (1997-2007).” Geophysical Research Letters, doi:10.1029/2010GL046167

Westberry, T., M. J. Behrenfeld, D. A. Siegel, and E. Boss. 2008. “Carbon-Based Primary Productivity Modeling with Vertically Resolved Photoacclimation.” *Global Biogeochemical Cycles* 22: GB2024. doi:10.1029/2007GB003078.

**Figure Captions**

Figure 1. (a and b) Maps of the 16-year averaged (1998-2013) monthly mean surface POC concentration in the months of a) February and b) July. (c and d). Coefficient of variation (CV) for the POC concentrations in the months of c) February and d) July.

Figure 2. a) Annual (1998-2013) time series (gray lines) and the 16-year averaged annual cycle (black line) of spatially averaged POC concentration in the North Atlantic, South Atlantic, North Pacific, South Pacific, Indian Ocean, Southern Ocean and global ocean, respectively. b) Example estimates of power spectral density obtained from the 16-year time series of surface POC concentrations. These power spectra are normalized by the total variance. c) The geographical variability of the values of peaks in the normalized power spectral density estimates (Gxn) in the annual period. d) The geographical variability of the values of peaks in the normalized power spectral density estimates (Gxn) in the semiannual period.

Figure 3. Summary of the 16-year averaged annual cycle of surface POC concentration: a) annual minimum, b) annual maximum c) day of the year when the minimum POC concentration is observed, d) day of the year when the maximum POC concentration is observed, e) amplitude of the annual cycle of POC concentration.

Figure 4. Inter-annual variability in regionally averaged mean annual POC concentrations (indicated as black dots). Solid lines are the linear regression estimates of the multi-year trends summarized in Table 1.

Figure 5. Example maps of the euphotic depth ($z_{eu}$, left side panel) and the mixed layer depth (MLD, right side panel) in February (a and b) and July (c and d).

Figure 6. Maps of the 16-year average water column POC biomass in February (left side panel) and July (right side panel): a and b) integrated in the euphotic depth ($POC_{Zeu}$), c

and d) integrated in the mixed layer ($POC_{MLD}$), e and f) $POC_{max}$ (see explanations in the text).

Figure 7. Annual (1998-2013) time series (gray lines) and the 16-year averaged annual cycle (black line) of spatially averaged $POC_{max}$ in the North Atlantic, South Atlantic, North Pacific, South Pacific, Indian Ocean, Southern Ocean and global ocean, respectively.

Figure 8. Summary of the 16-year averaged annual cycle of the water column integrated biomass: a) annual minimum $POC_{max}$, b) annual maximum $POC_{max}$, c) day of the year when the minimum $POC_{max}$ is observed, d) day of the year when the maximum $POC_{max}$ is observed, e) amplitude of the annual cycle of $POC_{max}$.

Figure 9. a) Comparison of the latitudinal changes in the day of the year when the annual maximum POC concentrations and $POC_{max}$ are observed, b) time series of the $POC_{max}$ and PP estimated with the VGPM model in the northern North Atlantic, c) time series of the MLD and surface POC concentration in the northern North Atlantic (region located between 60-46.7$^{o}$ N and 47-15$^{o}$ W).

Figure 10. Inter-annual variability in regionally averaged mean annual estimates of $POC_{max}$ (indicated as black dots). Solid lines are the linear regressions indicating the 16-year trends summarized in Table 1.

Figure 11. Maps indicating pixels with statistically significant ($p<0.05$, 95% confidence level) trend in the a) POC concentrations, b) water column integrated $POC_{Zeu}$, c) water column integrated $POC_{MLD}$, d) water column integrated $POC_{max}$. e) euphotic depth, f) mixed layer depth.

Figure 12. (Top panels) Example maps of the ratio of daily primary production and the 16-year averaged daily mean $POC_{max}$. Estimates are based on the a) VGPM and b) CBPM models. (Middle panels) Maps indicating pixels with statistically significant

($p<0.05$, 95% confidence level) trend in the ratios $PP/POC_{max}$ shown in panels a and b. (Bottom panels) Maps indicating pixels with statistically significant trend in the PP estimated with the e) VGPM and f) CBPM models.

## Figures

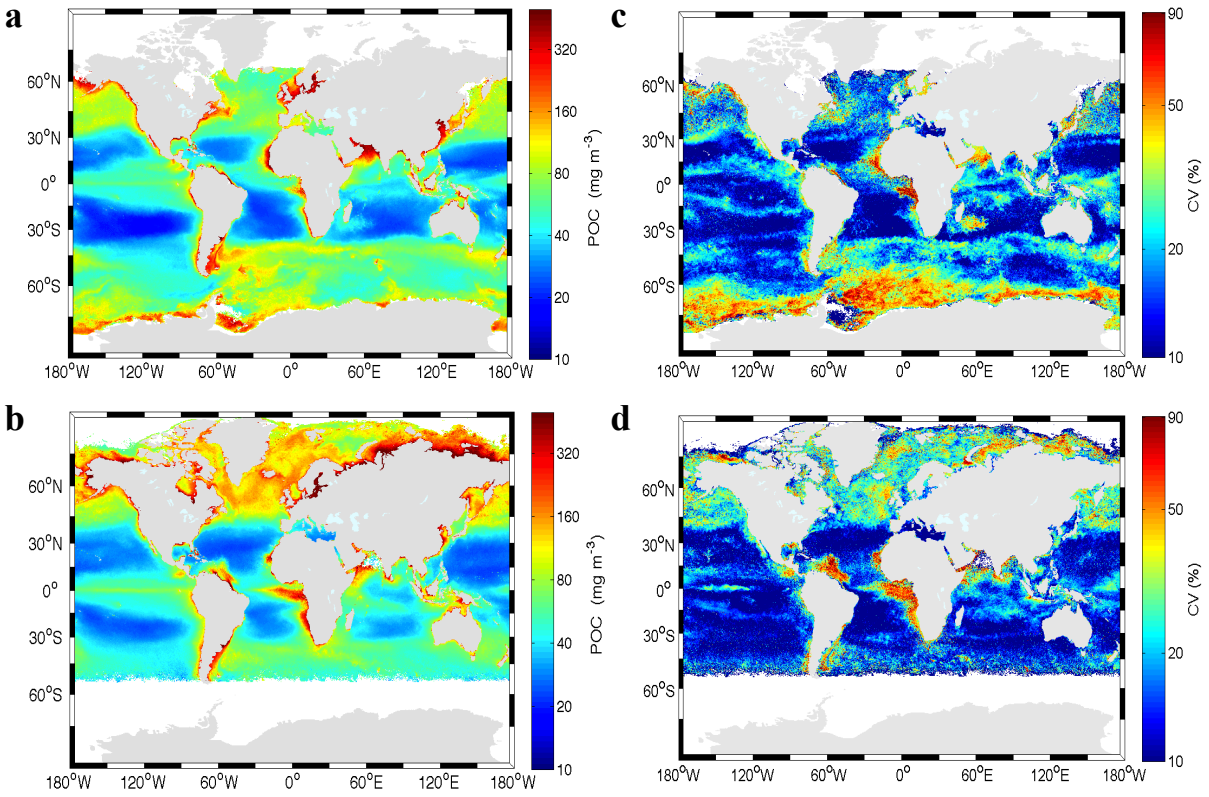


Figure 1. (a and b) Maps of the 16-year averaged (1998-2013) monthly mean surface POC concentration in the months of a) February and b) July. (c and d). Coefficient of variation (CV) for the POC concentrations in the months of c) February and d) July.

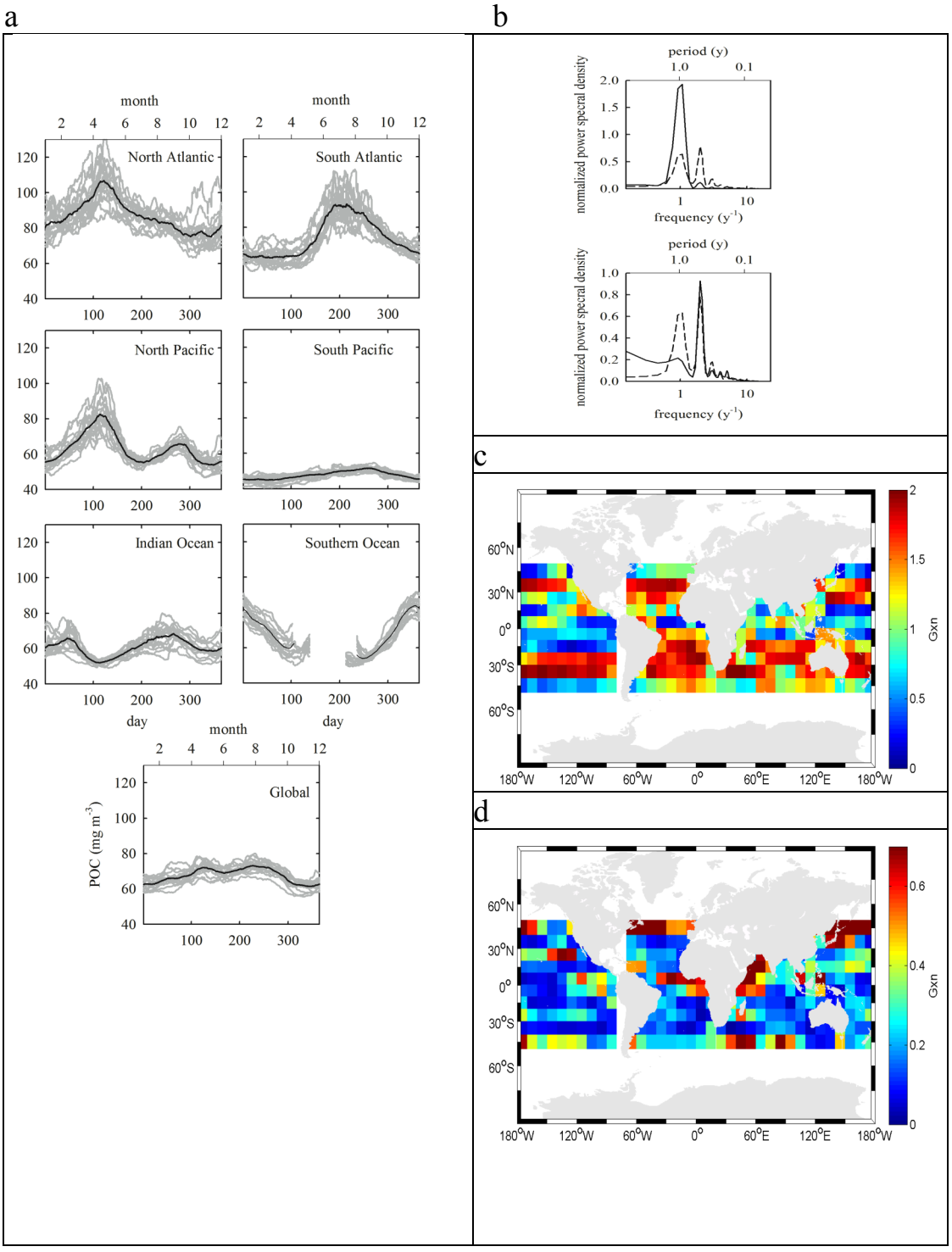


Figure 2. a) Annual (1998-2013) time series (gray lines) and the 16-year averaged annual cycle (black line) of spatially averaged POC concentration in the North Atlantic, South Atlantic, North Pacific, South Pacific, Indian Ocean, Southern Ocean and global ocean, respectively. b) Example estimates of power spectral density obtained from the 16-year time series of surface POC concentrations. These power spectra are normalized by the total variance. c) The geographical variability of the values of peaks in the normalized

power spectral density estimates (Gxn) in the annual period. d) The geographical variability of the values of peaks in the normalized power spectral density estimates (Gxn) in the semiannual period.

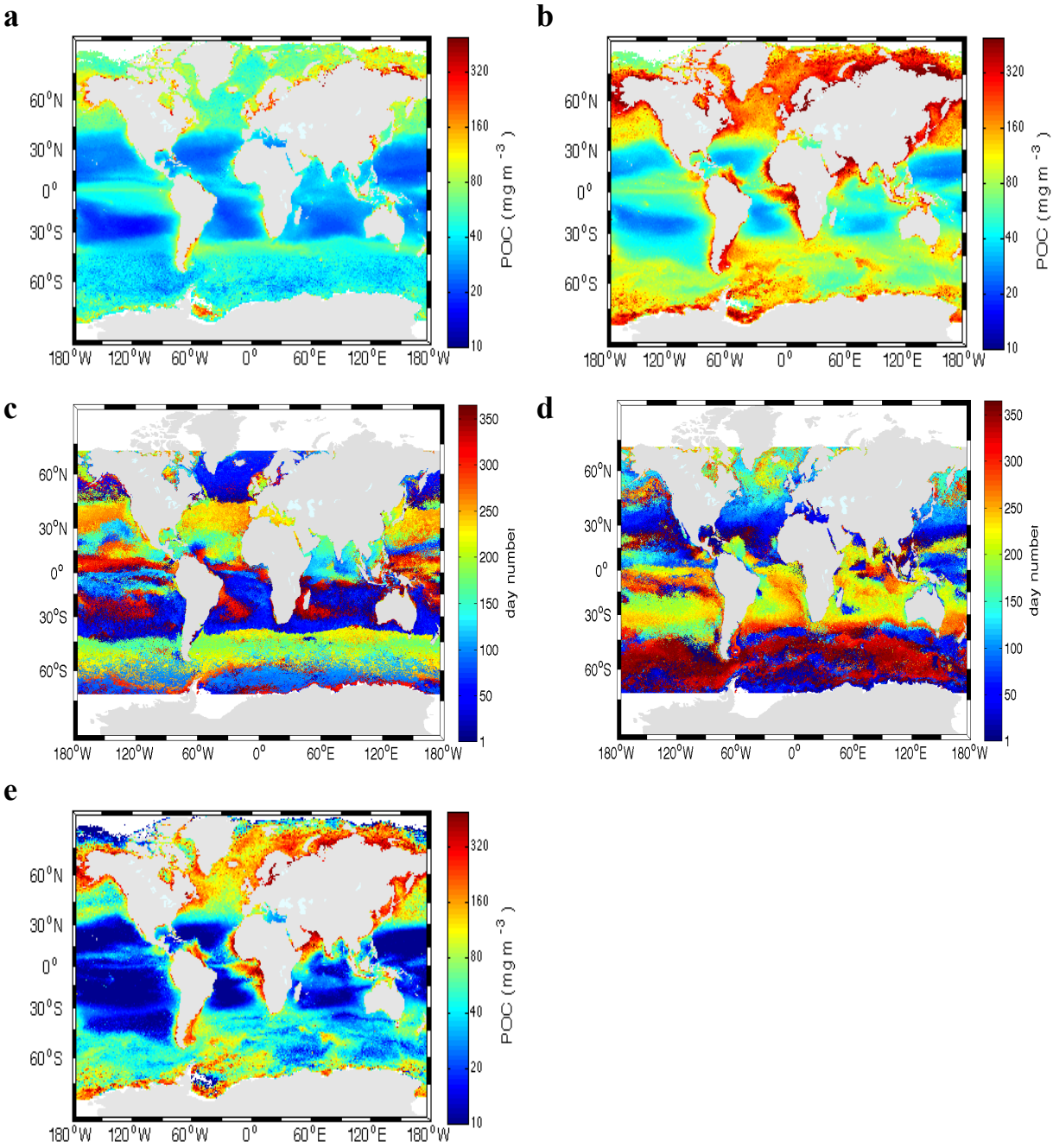


Figure 3. Summary of the 16-year averaged annual cycle of surface POC concentration: a) annual minimum, b) annual maximum c) day of the year when the minimum POC concentration is observed, d) day of the year when the maximum POC concentration is observed, e) amplitude of the annual cycle of POC concentration.

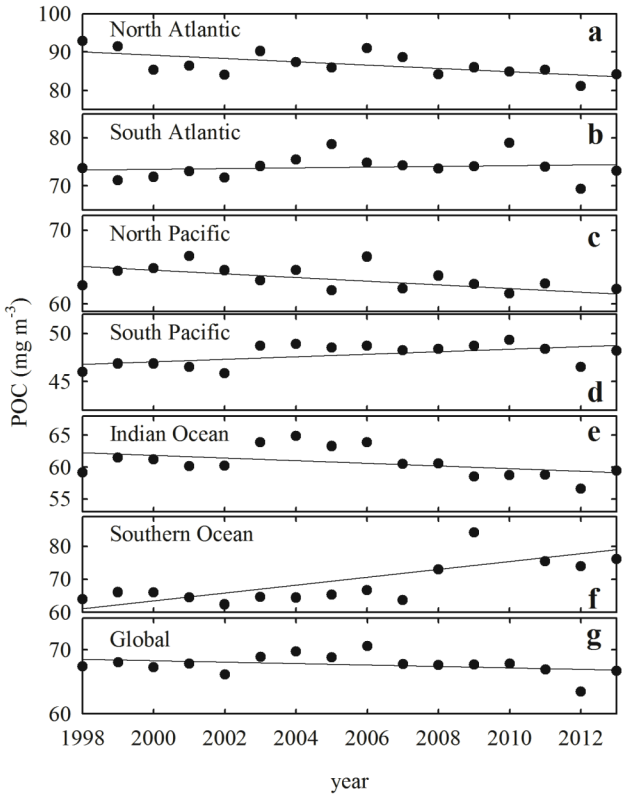


Figure 4. Inter-annual variability in regionally averaged mean annual POC concentrations (indicated as black dots). Solid lines are the linear regression estimates of the multi-year trends summarized in Table 1.

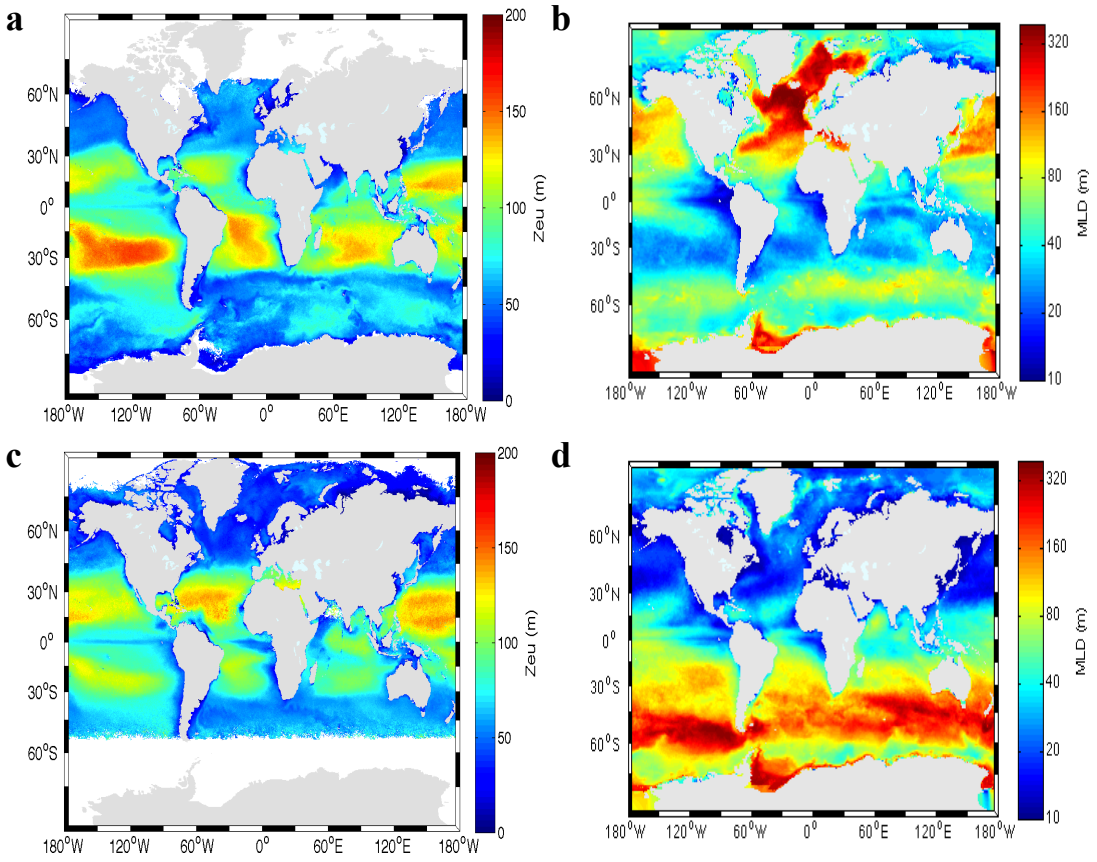


Figure 5. Example maps of the euphotic depth ($z_{eu}$, left side panel) and the mixed layer depth (MLD, right side panel) in February (a and b) and July (c and d).

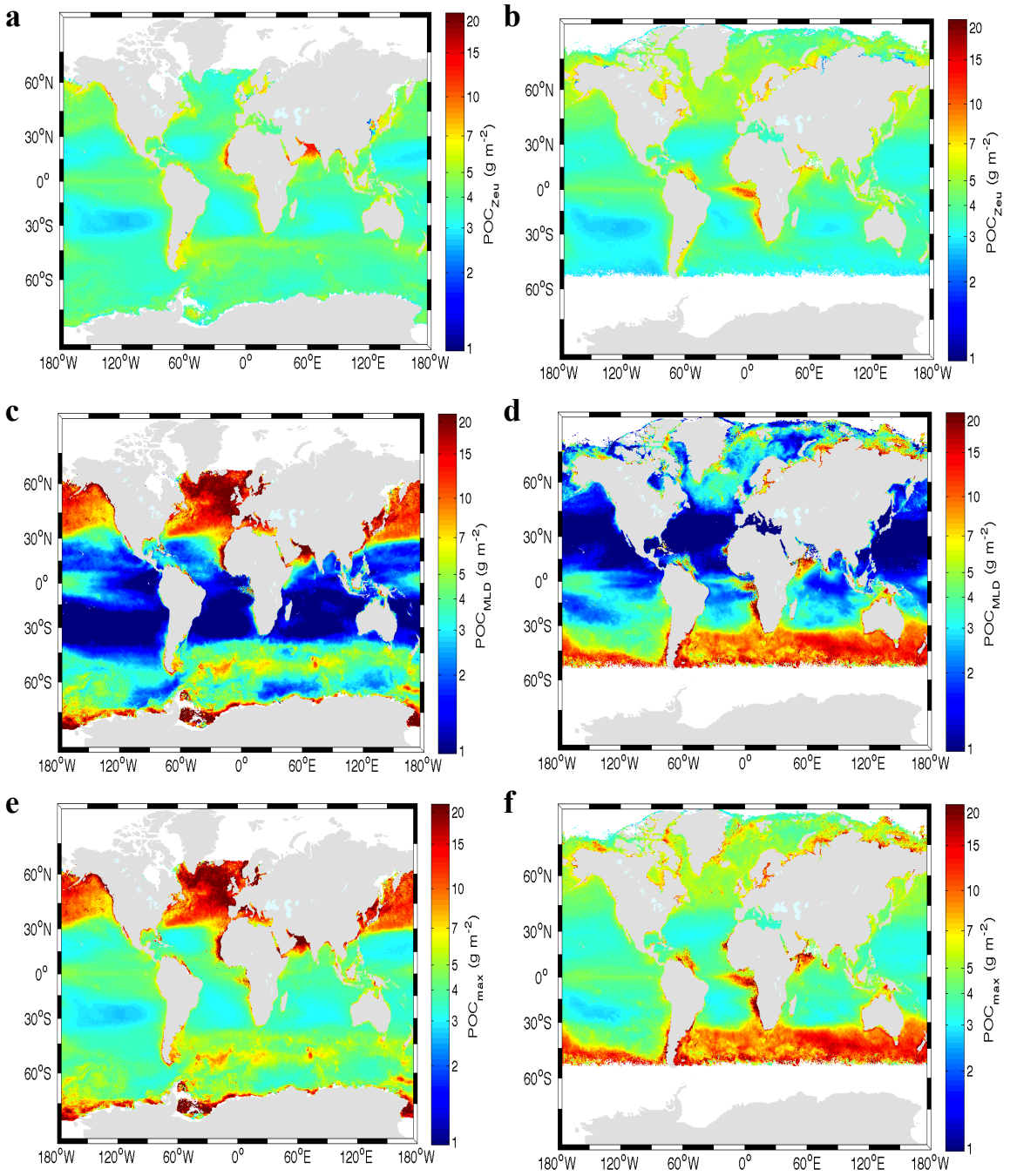


Figure 6. Maps of the 16-year average water column POC biomass in February (left side panel) and July (right side panel): a and b) integrated in the euphotic depth ($POC_{Zeu}$), c and d) integrated in the mixed layer ($POC_{MLD}$), e and f) $POC_{max}$ (see explanations in the text).

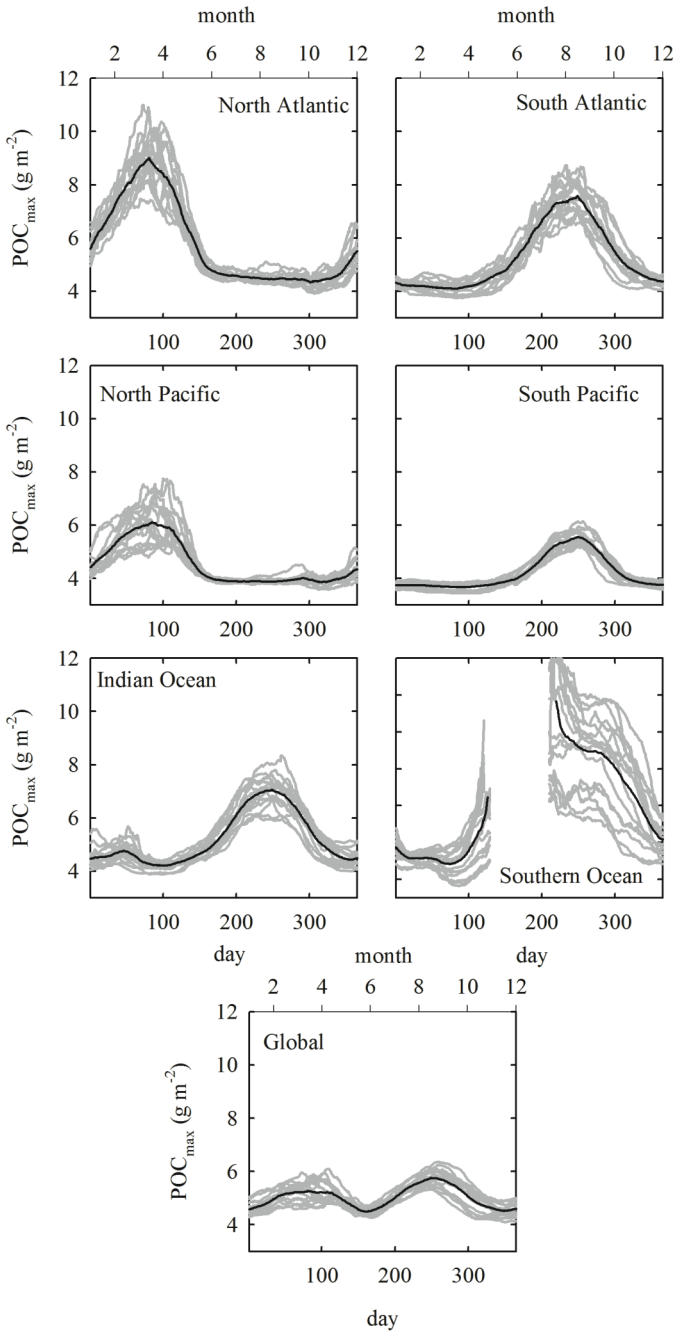


Figure 7. Annual (1998-2013) time series (gray lines) and the 16-year averaged annual cycle (black line) of spatially averaged $POC_{max}$ in the North Atlantic, South Atlantic, North Pacific, South Pacific, Indian Ocean, Southern Ocean and global ocean, respectively.

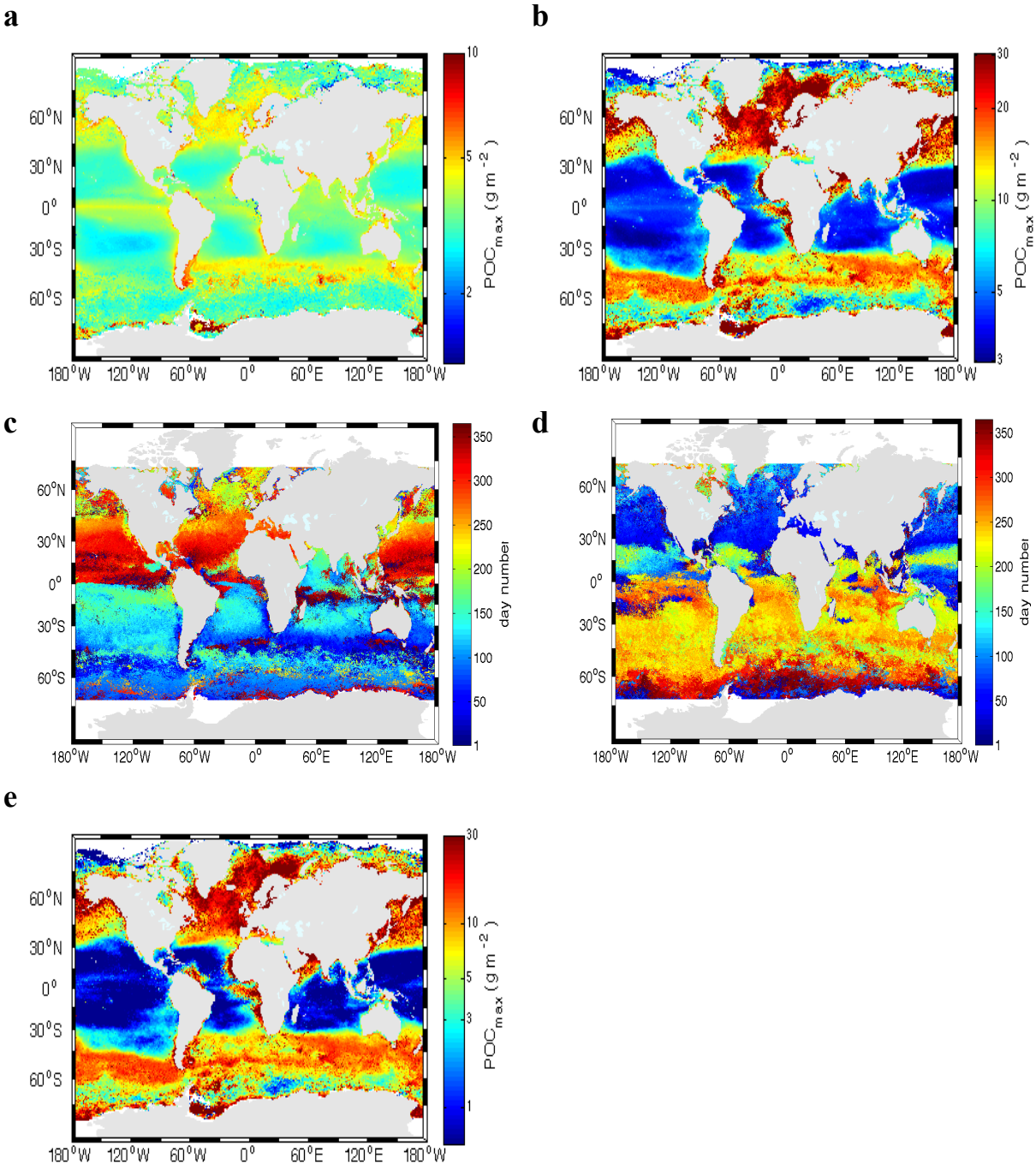


Figure 8. Summary of the 16-year averaged annual cycle of the water column integrated biomass: a) annual minimum $POC_{max}$, b) annual maximum $POC_{max}$, c) day of the year when the minimum $POC_{max}$ is observed, d) day of the year when the maximum $POC_{max}$ is observed, e) amplitude of the annual cycle of $POC_{max}$.

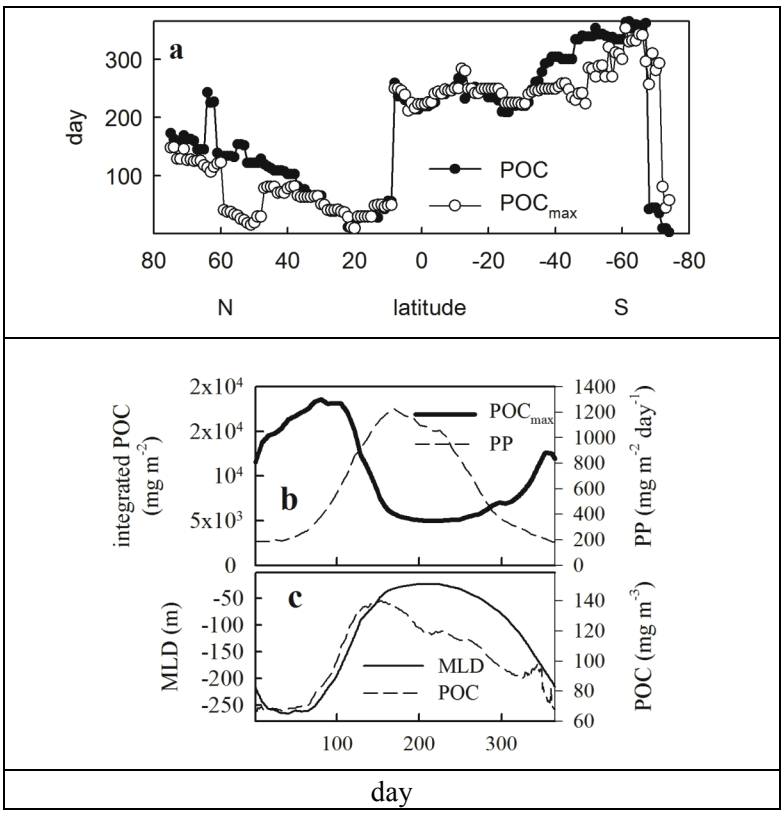


Figure 9. a) Comparison of the latitudinal changes in the day of the year when the annual maximum POC concentrations and $POC_{max}$ are observed, b) time series of the $POC_{max}$ and PP estimated with the VGPM model in the northern North Atlantic, c) time series of the MLD and surface POC concentration in the northern North Atlantic (region located between 60-46.7$^o$ N and 47-15$^o$ W).

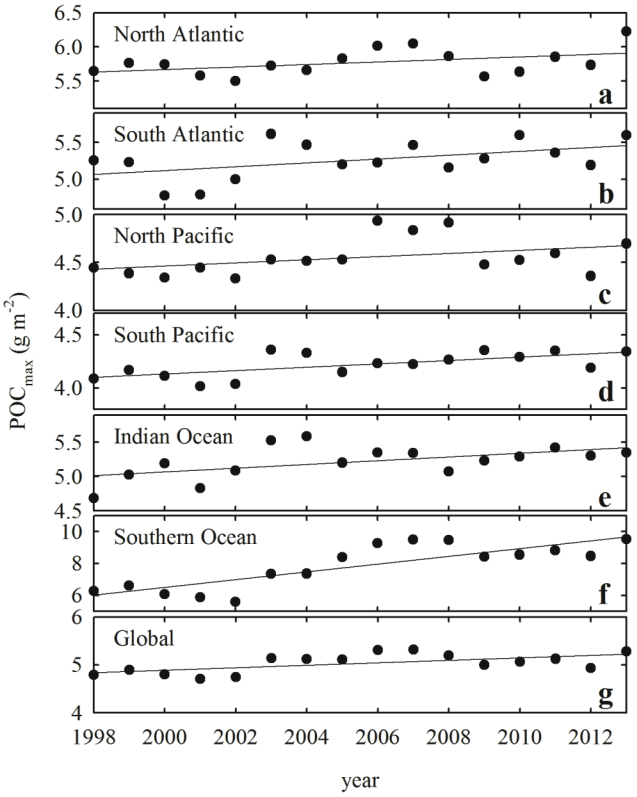


Figure 10. Inter-annual variability in the regionally averaged mean annual estimates of the $POC_{max}$ (indicated as black dots). Solid lines are the linear regressions demonstrating the 16-year trends summarized in Table 1.

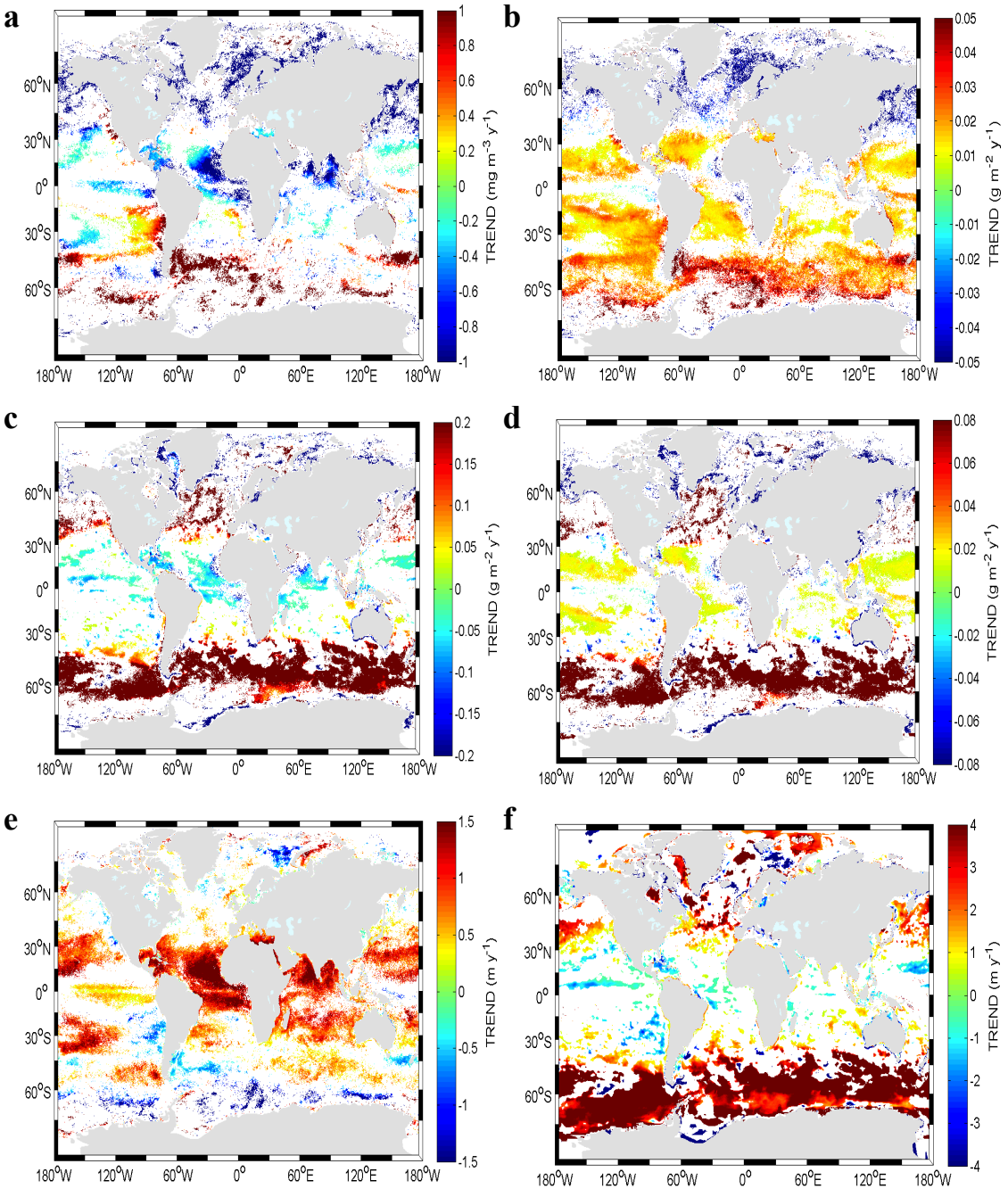


Figure 11. Maps indicating pixels with statistically significant ($p<0.05$, 95% confidence level) trend in the a) POC concentrations, b) water column integrated $POC_{Zeu}$, c) water column integrated $POC_{MLD}$, d) water column integrated $POC_{max}$, e) euphotic depth, f) mixed layer depth.

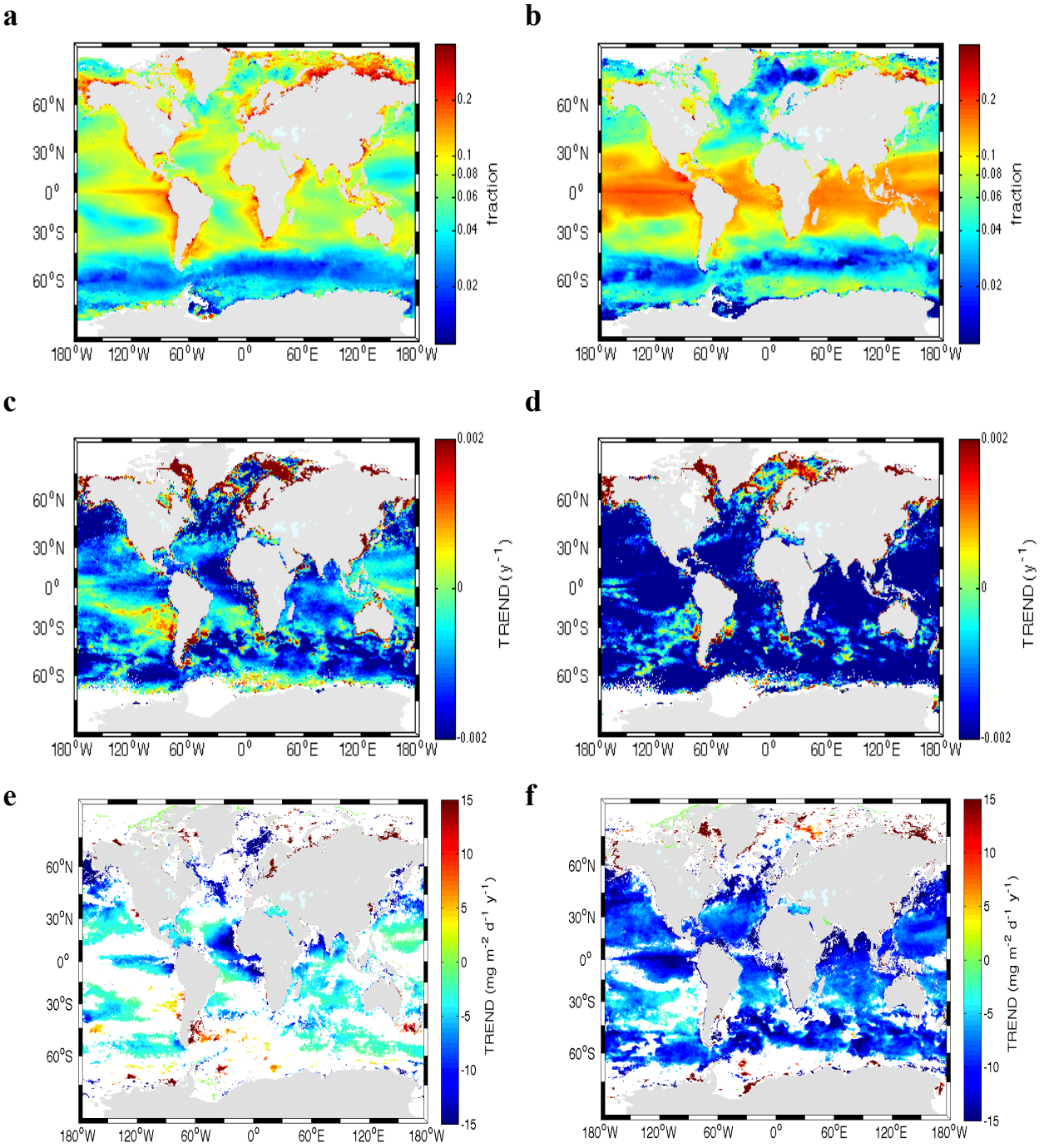


Figure 12. (Top panels) Example maps of the ratio of daily primary production and the 16-year averaged daily mean $POC_{max}$. Estimates are based on the a) VGPM and b) CBPM models. (Middle panels) Maps indicating pixels with statistically significant ($p<0.05$, 95% confidence level) trend in the ratios $PP/POC_{max}$ shown in panels a and b. (Bottom panels) Maps indicating pixels with statistically significant trend in the PP estimated with the e) VGPM and f) CBPM models.